Available online at www.sciencedirect.com
SCIENCE DIRECT
Journal of Catalysis 239 (2006) 200–211
JOURNAL OF CATALYSIS
www.elsevier.com/locate/jcat

Synthesis, characterization, and catalytic function of novel highly dispersed tungsten oxide catalysts on mesoporous silica

Jose E. Herrera [a], Ja Hun Kwak [a], Jian Zhi Hu [a], Yong Wang [a], Charles H.F. Peden [a,*], Josef Macht [b], Enrique Iglesia [b]

[a] *Institute for Interfacial Catalysis, Pacific Northwest National Laboratory, PO Box 999, MS K8-98, Richland, WA 99352, USA*
[b] *Department of Chemical Engineering, University of California, 103 Gilman Hall, Berkeley, CA 94720-1462, USA*

Received 13 September 2005; revised 24 January 2006; accepted 25 January 2006

Available online 28 February 2006

Abstract

The physical and chemical properties of tungsten oxide supported on SBA-15 mesoporous silica prepared by a controlled grafting process through atomic layer deposition (ALD) were studied using complementary characterization methods. X-ray diffraction, optical absorption, and transmission electron microscopy showed that tungsten oxide species are highly dispersed on SBA-15 surfaces, even at 30 wt% WO_x content (surface density, 1.33 WO_x/nm^2). ALD methods led to samples with much better thermal stability than those prepared via impregnation. Dehydration reactions of 2-butanol and methanol dehydration were used as probe reactions. Differences in reaction rates between the samples prepared by ALD and conventional impregnation may reflect the sintering resistance of catalysts prepared by ALD. Notably, temperature-programmed oxidation of spent catalysts showed that carbon formation was not responsible for the different dehydration rates in samples prepared by ALD and impregnation.

Keywords: Tungsten oxide; SBA–15; Methanol dehydration; 2-Butanol dehydration; DRS UV–vis; TEM; ^{1}H NMR; XRD; TPO

1. Introduction

Supported metal oxides are an important family of catalysts used in the petrochemical and refining industry. Catalytic reactions, such as ethylene polymerization, alkane oxidative dehydrogenation, alkene metathesis, and selective catalytic reduction of NO_x with ammonia, occur on supported metal oxides [1–7]. Many studies have addressed the structure and function of these catalytic materials, but the origins of their high activity remain the subject of active study. There is general consensus that active sites are of an acidic nature [8,9], but some studies suggest the possible involvement of redox cycles involving the reduction of metal oxide centers and radical-like intermediates [10].

Transition metal oxides with hexavalent and pentavalent cations have shown the highest activity for the aforementioned transformations. For some of these metal oxides, catalytic rates appear to be linked to the formation of strong Brønsted acid sites, which are stabilized by the effective delocalization of electron density in the conjugated base [11–13]. Among the transition metals with these characteristics, tungsten oxide gives the strongest Brønsted acid sites, either as bulk or supported oxides [14–18], but their structure and catalytic properties are strongly influenced by the support. Several studies have explored how interactions between support and tungsten oxide domains affect catalytic activity. Indeed, even for a given WO_x support system, WO_x domains exhibit a range of surface structures that depend strongly on synthetic protocols, such as the WO_x precursor and content, as well as on the thermal history of these materials [19–23].

Several reports have addressed the characterization of metal oxide-supported tungsten oxide species [16,24–27], and the specific nature of tungsten supported on ZrO_2 as acid cata-

* Corresponding author.
E-mail address: chuck.peden@pnl.gov (C.H.F. Peden).

0021-9517/$ – see front matter
doi:10.1016/j.jcat.2006.01.034

lysts for *o*-xylene isomerization [11–13] and butanol dehydration [28,29]. There are very few reports describing the use of mesoporous silica as a support for tungsten oxide species, however [30,31]. Zhang et al. described the synthesis of tungsten-containing MCM-41 with good dispersion, but segregated crystalline WO_3 was detected even after mild thermal treatments [32]. Briot et al. attempted to avoid crystalline phases by using oxoperoxometalate precursors that form at low pH in the presence of H_2O_2. The poor stability of these materials was evident from the extensive leaching of the tungsten species [33].

Here we report a novel method for grafting tungsten oxide species onto mesoporous silica (SBA-15) surfaces. This atomic layer deposition (ALD) method uses organic solvents and anhydrous conditions to control the deposition of tungsten oxide species onto the silica surface and to avoid the formation of WO_x oligomers prevalent in aqueous solutions at nearly neutral pH. The resulting improvements in dispersion and thermal stability of tungsten oxide species were confirmed using UV–vis light diffuse reflectance spectroscopy (DRS), X-ray diffraction (XRD), transmission electron microscopy (TEM), and magic-angle spinning (MAS) ^{1}H nuclear magnetic resonance (NMR). Methanol and 2-butanol dehydration were used as probe reactions. Temperature-programmed oxidation (TPO) and UV–vis spectra of spent samples were used to explore catalyst deactivation mechanisms and the effects of synthesis protocols on catalytic function.

2. Experimental

2.1. Catalyst synthesis

Mesoporous SBA-15 silica was prepared using a previously reported protocol [34]. The resulting BET surface area after treatment in air at 773 K for 4 h was ∼860 m^2/g, and the average pore size was ∼7 nm using the N_2 adsorption method. This sample was suspended in anhydrous toluene (Aldrich, 99.8%) and refluxed for 3 h in a N_2 atmosphere to remove physisorbed water. Tungsten precursor solutions were prepared by dissolving a given amount of WCl_6 (Aldrich, 99.9%) in ∼150 cm^3 of toluene at ambient temperature and then adding 20 cm^3 ethanol (Aldrich, anhydrous). The solution was then refluxed in N_2 until a wet pH paper strip indicated that HCl was no longer present in the nitrogen effluent. The suspension containing dehydrated mesoporous silica in toluene was added to the tungsten precursor solution after the latter was cooled to ambient temperature, and the mixture was refluxed overnight in N_2. The reaction mixture was cooled, filtered, and washed with toluene several times until optical absorption analysis of the washing solvent indicated that tungsten precursors were no longer present. The solids were then dried in ambient air at 393 K for 0.5 h. This sample is designated as "as-synthesized." The amount of WCl_6 added was varied to give 0.33–2.66 WO_x/nm^2 surface density on SBA-15. We assume that three Si–OH groups on SBA-15 react with each WCl_6, which corresponds to a full monolayer at ∼30 wt% WO_3, or 1.33 WO_x/nm^2. The density of Si–OH groups on the mesoporous silica has been estimated as 4.0 Si–OH/nm^2 [35]. Samples with 25% (0.33 WO_x/nm^2), 50% (0.66 WO_x/nm^2), 75% (1.00 WO_x/nm^2), and 100% (1.33 WO_x/nm^2) monolayer coverage were prepared. As-synthesized WO_x/SBA-15 silica samples were treated in flowing dry air (Airgas, zero grade, 1.7 $cm^3\,s^{-1}\,g_{cat}^{-1}$) at 673 and 773 K for 2 h. An additional sample with 200% (2.67 WO_x/nm^2) monolayer coverage was prepared by repeating the ALD process described above on a 1.33-WO_x/nm^2 sample after calcination. Two other samples were prepared by incipient wetness impregnation (RI) of SBA-15 with aqueous solutions of ammonium metatungstate (Aldrich, 99.99%) to give 1.00 and 1.33 WO_x/nm^2 surface densities. These samples were also treated for 3 h at 673 K in flowing dry air. After calcination, all catalysts obtained by ALD were analyzed by Fourier transform infrared spectroscopy to ensure that no organic residues remained on the samples.

2.2. XRD

XRD data were collected with a Philips PW3040/00 X'Pert MPD system equipped with a Cu source ($\lambda = 1.5406$ Å), a vertical Θ–Θ goniometer (220 mm radius), and focusing optics (Bragg–Brentano geometry). The in situ experiments were performed using a heated stage equipped with an Anton Paar HTK 1200 oven. The samples were mounted within an alumina cavity-type holder (18 mm diameter) for analysis. Diffraction data were analyzed using JADE (Materials Data, Livermore, CA) and the Powder Diffraction File database (2003 Release, International Center for Diffraction Data, Newtown Square, PA).

2.3. TEM

TEM micrographs were obtained using a JEOL 2010 high-resolution analytical electron microscope operating at 200 kV. An energy-dispersive X-ray (EDX) analyzer was used for elemental analysis. Samples were dispersed using 2-propanol (Aldrich, 99.5%) onto a carbon-coated copper grid.

2.4. ^{1}H NMR

Solid-state ^{1}H NMR spectra were measured using a Varian/Chemagnetics CMX Infinity 300 MHz NMR device equipped with a Varian/Chemagnetics 7.5 mm HX MAS probe, operating at a spectral frequency of 299.98 MHz. All spectra were externally referenced to tetramethylorthosilicate at 0 ppm and were obtained using a 1-s recycle delay and a 5-kHz spinning rate.

2.5. UV–vis spectroscopy

UV–vis spectra were measured in diffuse reflectance mode using a Varian Cary 5G UV–vis–NIR spectrophotometer with an internal integration sphere. Powder samples were placed within a quartz cell, and spectra were measured in the region of 200–800 nm after drying ex situ at 343 K. A halon white (PTFE) reflectance standard was used for background subtraction unless otherwise indicated. Spent catalysts were first treated in flowing air (Airgas, zero grade) at 673 K to remove

carbon deposits, and then directly transferred from the reaction chamber to a He glove bag, from which they were loaded into sealed quartz cells to avoid exposure to ambient moisture. In situ measurements were performed on a Varian (Cary 4) spectrometer with a Harrick Scientific diffuse reflectance attachment (DRP-XXX) and a controlled environment chamber (DRA-2CR). Samples were treated in 20% O_2–He (Praxair, 99.999%, 0.83 $cm^3\,s^{-1}$) at 673 K and cooled in the same mixture to ambient temperature before spectra were measured. UV–vis spectra were also recorded on similarly treated samples during steady-state 2-butanol dehydration [0.5 kPa 2-butanol, He (Praxair, UHP grade, 1.33 $cm^3\,s^{-1}$)] at 423 K; MgO was used as a reflectance standard.

2.6. Catalytic rate measurements

Catalytic rates and selectivities were measured to evaluate dehydration of 2-butanol and methanol reactants. 2-Butanol dehydration rates were measured at 373 K in a quartz flow reactor (1.0 cm i.d.) using samples (0.020–0.050 g) dispersed onto a quartz frit. All samples were treated in flowing dry air (Airgas, zero grade, 0.8 $cm^3\,s^{-1}$) at 673 K for 1 h before catalytic measurements. Liquid 2-butanol (Aldrich, 99.5%, anhydrous) was vaporized into flowing He (Praxair, UHP, 0.3–5.3 $cm^3\,s^{-1}$) at ambient pressure and 373 K using a syringe pump to give 0.5 kPa 2-butanol. Reactant conversions were varied by changing the He flow rate (0.3–5.3 $cm^3\,s^{-1}$) at constant 2-butanol pressures (0.5 kPa). Reactant and product concentrations were measured by gas chromatography (GC), using a Hewlett-Packard 6890 gas chromatograph with a 50-m HP-1 methyl silicone capillary column and a flame ionization detector. Methanol dehydration rates were measured at 573 K using the same protocols as for 2-butanol. Liquid methanol (Aldrich, 99.9%, anhydrous) was vaporized into flowing He (Airgas, UHP) using a syringe pump to give 1 kPa of methanol. Reactant conversion was varied by changing the He flow rate (0.6–8.3 $cm^3\,s^{-1}$) at constant methanol pressure (1.0 kPa). Products were analyzed by on-line GC using an Agilent 3000 micro gas chromatograph equipped with a thermal conductivity detector and a Plot Q column. All dehydration rates are reported on the basis of the number of W atoms in each sample.

2.7. TPO

TPO measurements were carried out by passing a continuous flow (0.25 $cm^3\,s^{-1}$) of 2% O_2/He (Airgas 99.99%) over samples used for methanol dehydration as the temperature was increased linearly at 0.2 $K\,s^{-1}$ to 1073 K. The CO_2 and CO thus formed were quantitatively converted to methane in a methanator by mixing the effluent with 0.83 $cm^3\,s^{-1}$ H_2 and passing over a 15% Ni/Al_2O_3 catalyst held at 673 K. CH_4 formation rates were measured by a flame ionization detector (SRI model 110), calibrated with 100-μl pulses of CO_2 and by combustion of known amounts of graphite.

3. Results and discussion

3.1. XRD

The XRD patterns of WO_x/SBA-15 (1.33 W/nm^2) prepared by ALD and treated in dry flowing air at 673 and 773 K are shown in Fig. 1, together with those for SBA-15 and for WO_x/SBA-15 (1.33 W/nm^2) prepared by conventional impregnation (RI). The (100), (110), and (200) low-angle diffraction lines, corresponding to hexagonal mesoporous silica, are evident in all samples, indicating that the nearly amorphous materials are characterized by a short-range order. These data show that the SBA-15 mesoporous structure was retained after WO_x deposition and treatments at temperatures up to 773 K. No other diffraction lines were detected, indicating that crystalline WO_3 was not formed even after the samples were treated with high WO_x content at 773 K. In contrast, impregnated samples (Fig. 1b, top pattern) showed some diffraction lines at higher

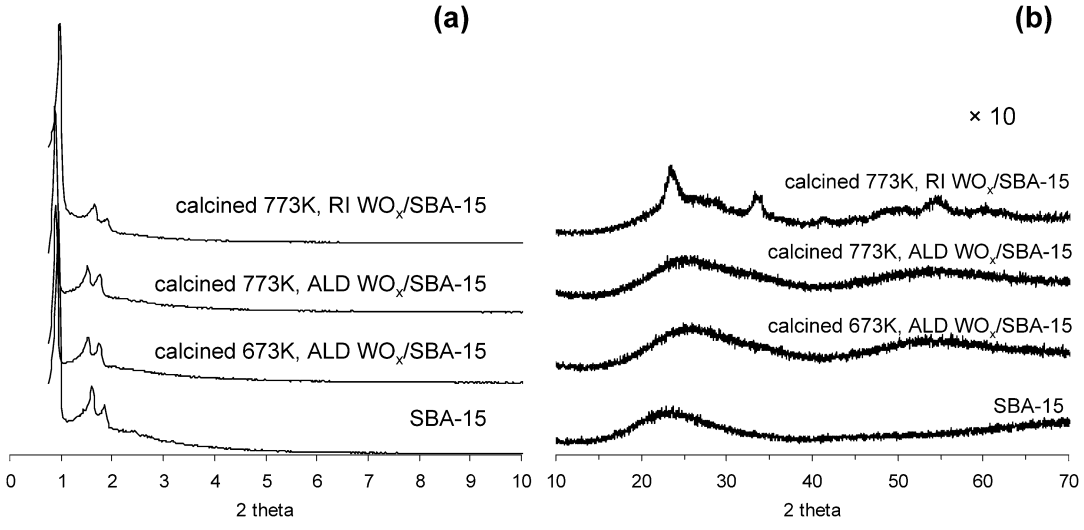

Fig. 1. X-Ray diffraction patterns obtained for SBA-15, ALD-WO_x/SBA-15 (1.33 WO_x/nm^2) calcined at 673 K, ALD-WO_x/SBA-15 (1.33 WO_x/nm^2) calcined at 773 K, and impregnated WO_x/SBA-15 (1.33 WO_x/nm^2) calcined at 773 K.

angles, corresponding to crystalline WO_3 ($2\theta = 23.1°, 23.6°$, and 24.4 °) [36].

3.2. TEM

TEM micrographs (at various sample orientations) of WO_x/SBA-15 prepared via different methods and with a range of WO_x contents and thermal treatments are shown in Figs. 2–4. These micrographs show well-ordered hexagonal arrays of one-dimensional mesopores typical of SBA-15 (Fig. 2a) for all samples [37]. WO_3 crystallites are not present at external SBA-15 surfaces in samples prepared by atomic layer deposition (Figs. 2 and 3), indicating that WO_x species are well dispersed in these samples even at 30 wt% WO_3 (1.33 WO_x/nm^2).

Fig. 2 shows TEM micrographs for WO_x/SBA-15 with a 1.33 W/nm^2 surface density prepared by atomic layer deposition after thermal treatments at 393, 673, and 773 K. Samples treated at 673 K are indistinguishable from the SBA-15 support or the untreated sample. Even after treatment at 773 K (Fig. 2d), no WO_3 clusters are detected. Samples prepared by impregnation methods (Fig. 4a) show WO_3 crystallites larger than 10 nm throughout the mesoporous silica structure after impregnation and drying and even before thermal treatment. In these samples, thermal treatment causes further crystallite growth; WO_3 structures of submicron size are evident in these samples after treatment at 673 or 773 K, consistent with the crystalline WO_3 phases detected by XRD (Fig. 1b, top diffraction pattern).

3.3. In situ XRD studies

The structural stability of WO_x/SBA-15 materials was also examined by in situ XRD during thermal treatment of a sample prepared by ALD (1.33 WO_x/nm^2) in air (Fig. 5). No crystalline WO_3 phases were detected at temperatures up to 823 K. At higher temperatures, some diffraction lines appeared, the intensity of which increased with increasing treatment temperature. Comparison with previously published patterns (Joint Committee on Powder Diffraction Standards JCPDS 83-0951) shows that these lines correspond to crystalline WO_3 species, a conclusion confirmed by TEM analysis and UV–vis spectroscopy. It is noteworthy that even at the highest temperature (1023 K), we still observed the low-angle diffraction lines (not shown), implying that the mesoporous structure of the hexagonal mesoporous silica was retained.

3.4. Solid-state ^1H NMR

High-resolution ^1H NMR spectroscopy (combining rotation and multiple-pulse spectroscopy [CRAMPS] [38] and MAS techniques) has been extensively used to characterize silica, alumina, and silica–alumina structures [39–42]. MAS-only spectra obtained for silica and zeolites are very similar to those obtained by more technically challenging CRAMPS techniques, because of the rather weak ^1H–^1H dipolar interactions in these systems [43]. This makes MAS-only techniques at-

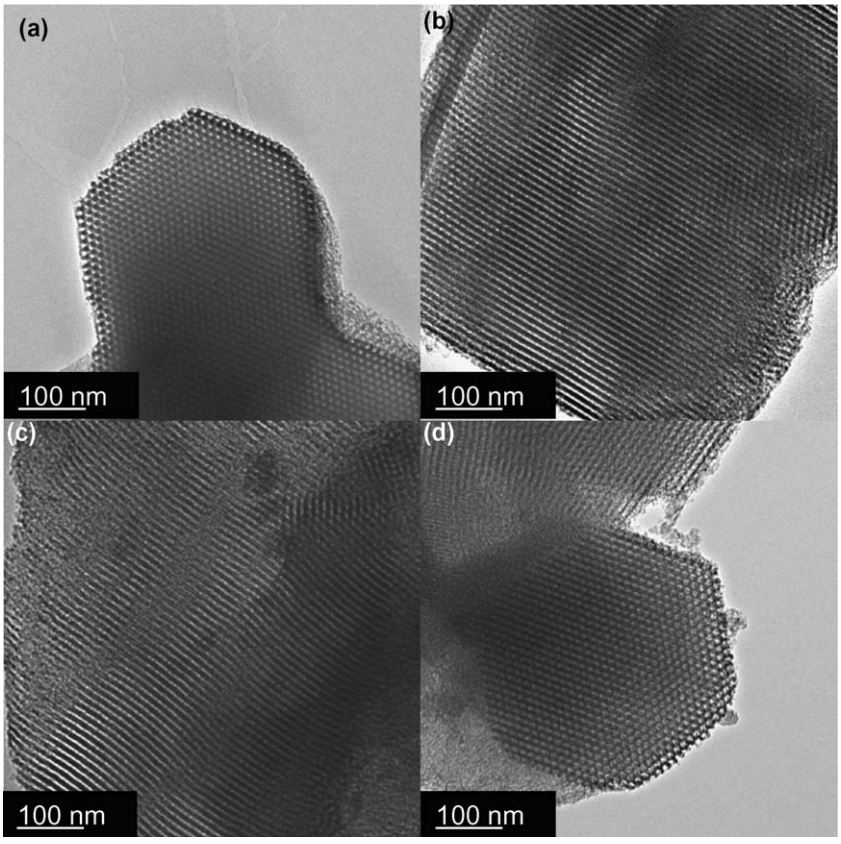

Fig. 2. TEM micrographs obtained for (a) SBA-15, (b) WO_x/SBA-15 (1.33 WO_x/nm^2) as-synthesized, (c) calcined at 673 K, and (d) calcined at 773 K. The last three samples were prepared by atomic layer deposition.

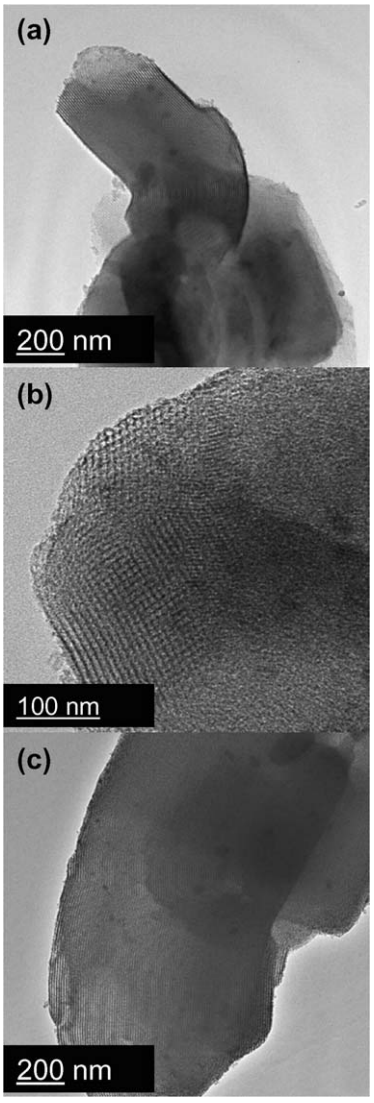

Fig. 3. TEM micrographs obtained for WO_x/SBA-15 samples with different tungsten oxide loadings: (a) 0.33 WO_x/nm^2, (b) 0.66 WO_x/nm^2, and (c) 1.00 WO_x/nm^2. All three samples were prepared by atomic layer deposition and were calcined at 673 K before analysis.

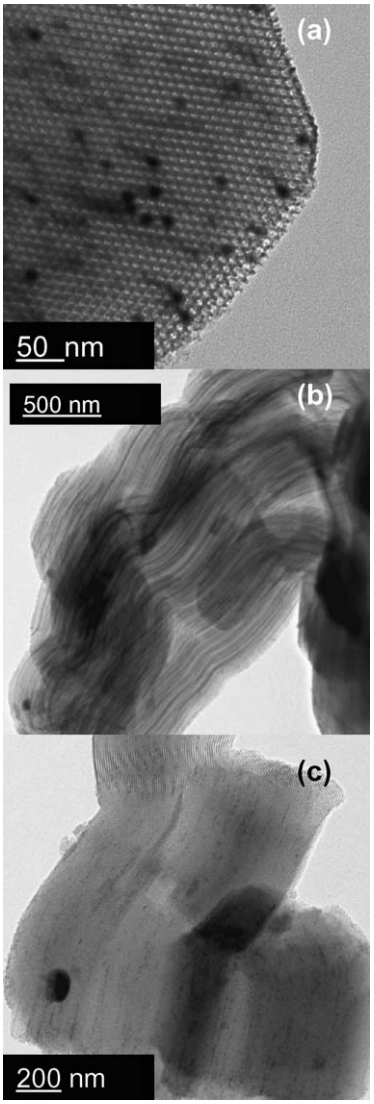

Fig. 4. TEM micrographs obtained for a WO_x/SBA-15 (1.33 WO_x/nm^2) catalyst prepared by conventional impregnation, (a) and (b) calcined at 673 K and (c) calcined at 773 K.

tractive for characterizing surface protons in high-surface area materials, including heterogeneous catalysts.

^{1}H NMR–MAS spectra of ALD-synthesized WO_x/SBA are shown in Figs. 6 and 7. Fig. 6 shows spectra for pure SBA-15 mesoporous silica (a), for "as synthesized" 1.33 W/nm^2 WO_x-SBA-15 (b), and for the latter after treatment in air at 673 K (c) and 773 K (d). The NMR spectrum for pure SBA-15 shows a broad line centered at ∼3.5 ppm and a very sharp line at ∼1.6 ppm, the latter reflecting the presence of isolated silanols (Si–OH) [44]. The broad line at ∼3.5 ppm (Fig. 6a) is assigned to protons in H_2O and Si–OH interacting with each other via hydrogen bonding [45].

Four ^{1}H NMR lines were observed in the "as synthesized" WO_x-SBA-15 sample with 1.33 W/nm^2 surface density (Fig. 6b), with chemical shifts at 0.75, 2.0, 3.5, and 6.9 ppm. Toluene was used as a solvent for synthesis; thus, a ^{1}H MAS–NMR spectrum was measured for pure SBA-15 impregnated with toluene. This demonstrates that the 2.0 and 6.9-ppm lines arise from methyl and aromatic protons, respectively, in residual toluene. The line at 3.5 ppm arises from hydrogen-bonded hydroxyl groups and/or physisorbed water, as in pure SBA-15. In contrast with pure SBA-15, the line at 1.6 ppm (Si–OH) was not observed in the spectra of 1.33 W/nm^2 WO_x-SBA-15. Instead, a sharp line was detected at 0.75 ppm, which is assigned to water molecules that are hydrogen-bonded to W–OH groups based on quantum chemistry calculations at the density function level. The details of these calculations will be published in a separate report. This assignment was confirmed by increasing the tungsten content, which led to the concurrent disappearance of the line for Si–OH groups and appearance of the 0.75-ppm line, demonstrating the titration of silanols in SBA-15 by tungsten species.

Fig. 6c shows NMR spectra after treatment at 673 K in dry air. Three sharp lines are observed at 0.75, 1.61, and 3.5 ppm. The reappearance of Si–OH protons (at 1.61 ppm) indicates that thermal treatment causes the coalescence of some grafted WO_x species to form WO_3 clusters, which, however, remain highly

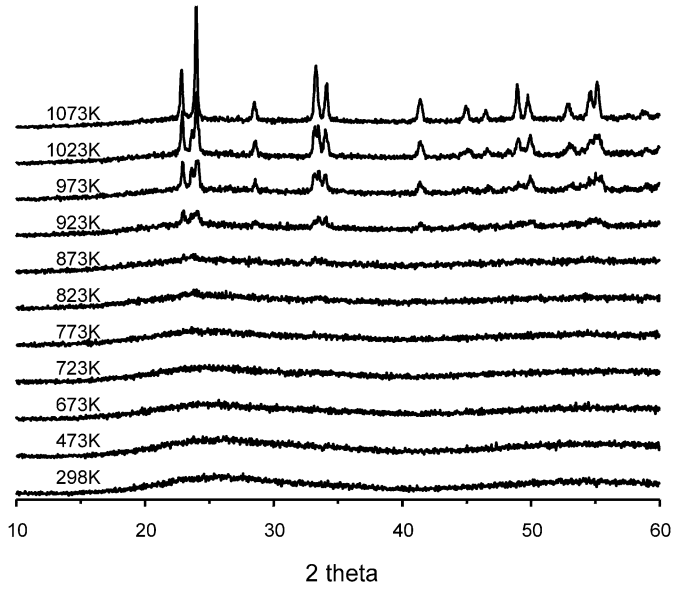

Fig. 5. X-Ray diffraction patterns obtained on a ALD-WO_x/SBA-15 (1.33 WO_x/nm^2) catalyst prepared by atomic layer deposition. The diffractograms were obtained in situ during thermal treatment at the indicated temperatures.

dispersed (see the discussion on UV–vis spectra below). This change in WO_x morphology leads in turn to domains of bare silica with isolated Si–OH at the surface. In contrast, treatment in air at 773 K (Fig. 6d) leads to the disappearance of the 0.75-ppm line with only the silanol line remaining in the NMR spectrum. This dehydroxylation process of the WO_x species reflects, at least in part, the formation of W–O –W bonds, as discussed below.

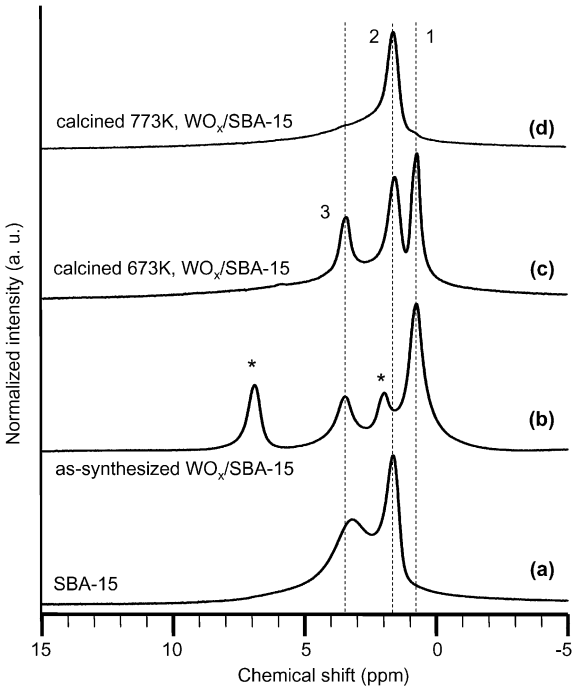

Fig. 6. ^{1}H NMR MAS spectra of (a) SBA-15 and of ALD-WO_x/SBA-15 (1.33 WO_x/nm^2) after subsequent treatments: (b) as-synthesized, (c) calcined at 673 K, and (d) calcined at 773 K. The peaks at 2.0 and 6.9 ppm in spectrum (b) correspond to methyl and aromatic protons of residual toluene respectively.

Fig. 7 shows ^{1}H NMR–MAS spectra for four WO_x-SBA-15 samples of varying W content treated in air at 673 K. The intensity of the line at 0.75 ppm (assigned to water molecules that are hydrogen-bonded to W–OH protons) increases with increasing W content, and the intensity ratio of the line at 0.75 ppm relative to the 1.61-ppm line (Si–OH protons) increases concurrently. This confirms the consumption of the silanol groups via reaction with tungsten oxide species with increasing WO_x content. In addition, the relatively high concentration of tungsten hydroxyl groups is consistent with highly dispersed tungsten oxide species. Indeed, if a significant amount of crystalline tungsten oxide clusters were to form via condensation processes that yield W–O–W linkages, then the value of the ratio of the intensity of the peak at 0.75 ppm to that at 1.6 ppm would dramatically decrease; however, this is not observed even for the samples with surface density of 1.33 W/nm^2 (30 wt% WO_3). As for W–OH protons, the intensity of the sharp water peak at 3.5 ppm increases in parallel with that of molecules that are hydrogen-bonded to tungsten hydroxyl protons at 0.75 ppm, and the ratio of the peak intensity at 3.5 ppm relative to that at 0.75 ppm is nearly constant (0.57 ± 0.02), indicating that this water peak also may be associated with the tungsten hydroxyl protons rather than with the silanol groups. Further investigation is needed to understand the exact nature of this peak.

3.5. UV–vis spectroscopy of fresh samples

The absorption edge energy in the UV–vis spectra is a useful indicator of the dispersion and local structure of transition metal cations in oxide domains [13,46–48]. Several methods

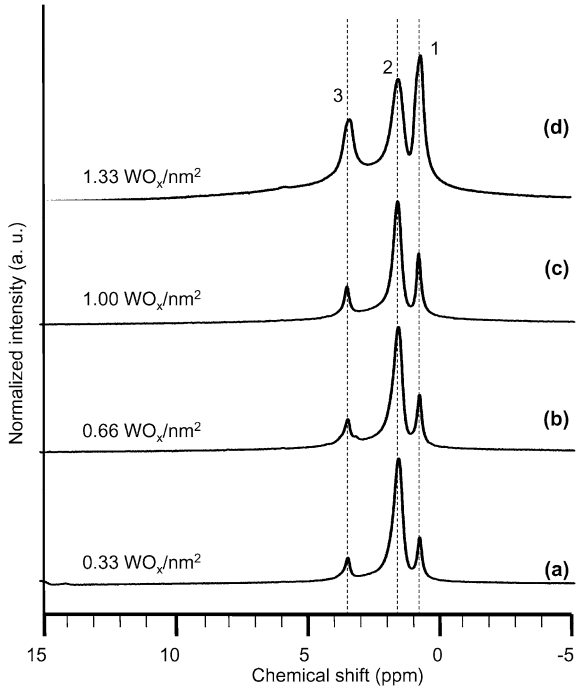

Fig. 7. Variation of ^{1}H NMR MAS spectra with tungsten oxide loading on WO_x/SBA-15 catalysts prepared by atomic layer deposition: (a) 0.33 WO_x/nm^2, (b) 0.66 WO_x/nm^2, (c) 1.00 WO_x/nm^2, and (d) 1.33 WO_x/nm^2. All samples were calcined at 673 K before analysis.

for estimating the band gap energy of tungsten oxide compounds using optical absorption spectroscopy have been proposed. Davis and Mott [49] proposed an expression to relate the absorption coefficient and the photon energy for various types of electronic transitions prevalent in semiconductors. For dispersed WO_x domains, Barton et al. [13] used the square root of the Kubelka–Munk function multiplied by the photon energy, which allows the edge energy to be obtained by extrapolation to zero absorbance for amorphous semiconductors. The values thus obtained carry information about the average domain size of the oxide nanoparticles [50], although the values also depend on local symmetry [51] and support electronegativity [29].

Diffuse-reflectance UV–vis spectra are shown in Fig. 8 for the WO_x-SBA-15 samples. The absorption edge arises from ligand-to-metal charge transitions [52–54]. The position of the absorption edge allows comparisons between the samples reported here and reference compounds with known domain size, although such comparisons are not always straightforward. For instance, based on previously published X-ray absorption studies [55] and earlier extended Hückel calculations [56], Barton et al. [13] showed that for zirconia-supported WO_x catalysts, edge energy values >3.5 eV indicate the presence of isolated WO_x species in distorted octahedral symmetry and without bridging W–O–W bonds.

Table 1 shows absorption edge energies for several WO_x species of known domain size and coordination, together with those for SBA-15-supported WO_x samples prepared via ALD and impregnation methods with various tungsten contents and thermal treatments. Edge energies for all samples (3.0–3.8 eV) except the sample treated at 1073 K resemble those for $(NH_4)_{10}W_{12}O_{41}$, indicating that the WO_x domains are very small. The edge energy value decreases systematically with increasing WO_3 content and thermal treatment (Fig. 8), consistent with a parallel increase in WO_x domain size.

Fig. 8b shows the effect of thermal treatment temperature on the UV–vis spectra of 1.33 W/nm^2 WO_3-SBA-15. As for the samples in Fig. 8a, edge energy values of ∼3.1 eV indicate highly dispersed WO_x species. The shift to lower energies for the sample treated at 773 K is consistent with the growth of WO_x domains, probably via condensation reactions of W–OH to form W–O–W linkages. Indeed, ^{1}H NMR data show that W–OH groups disappear when the catalyst is treated above 773 K. The dispersion of this sample is relatively high, but treatment at 1073 K leads to the appearance of a low-energy shoulder (at 2.6 eV) near the absorption edge, corresponding to the formation of large WO_3 crystallites, also detected in this sample by XRD. The residual edge at higher energies indicates that some WO_x species remain reasonably well dispersed even after treatment at 1073 K.

Table 1
Edge energy values for different WO_x/SBA-15 catalysts obtained from the optical absorption spectra. The values obtained for samples of known domain size are also included for reference

Sample	Thermal treatment (K)	Edge energy value (eV)
WO_3	–	2.4 eV
$(NH_4)_{10}W_{12}O_{41}$	–	3.0 eV
Na_2WO_4	–	4.6 eV
WO_x/SBA-15 0.33 WO_x/nm^2	673 K	3.8 eV
WO_x/SBA-15 0.66 WO_x/nm^2	673 K	3.5 eV
WO_x/SBA-15 1.00 WO_x/nm^2	673 K	3.6 eV
WO_x/SBA-15 1.33 WO_x/nm^2	673 K	3.2 eV
WO_x/SBA-15 2.66 WO_x/nm^2	673 K	3.0 eV
WO_x/SBA-15 1.33 WO_x/nm^2	773 K	3.1 eV
WO_x/SBA-15 1.33 WO_x/nm^2	1073 K	3.0 and 2.6 eV
RI WO_x/SBA-15 1.00 WO_x/nm^2	673 K	3.5 eV
RI WO_x/SBA-15 1.33 WO_x/nm^2	673 K	3.1 eV

3.6. Catalytic dehydration of 2-butanol and methanol

The dehydration of 2-butanol and methanol reactions were used to probe the catalytic properties of WO_x-SBA-15 samples prepared via ALD and impregnation methods. Only dehydration products were detected for both alcohols (1-butene, *cis*- and *trans*-2-butenes, dimethyl-ether). Bimolecular dehydration

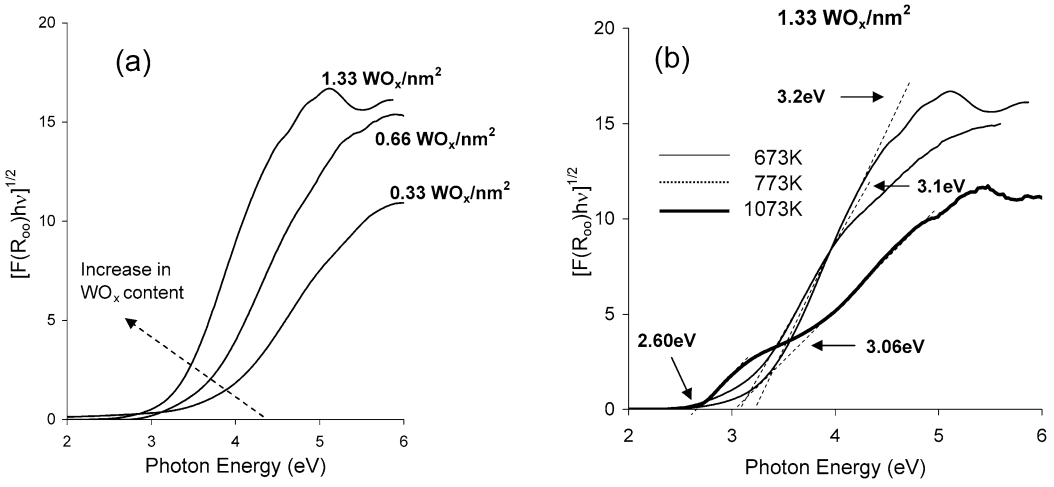

Fig. 8. (a) UV–vis DRS spectra for three WO_x/SBA-15 samples calcined at 673 K and with different tungsten loadings. (b) UV–vis DRS spectra for a WO_x/SBA-15 (1.33 WO_x/nm^2) sample after subsequent thermal treatments. All samples were prepared by atomic layer deposition. $[F(R_\infty)h\nu]$ represents the Kubelka–Munk function multiplied by the photon energy.

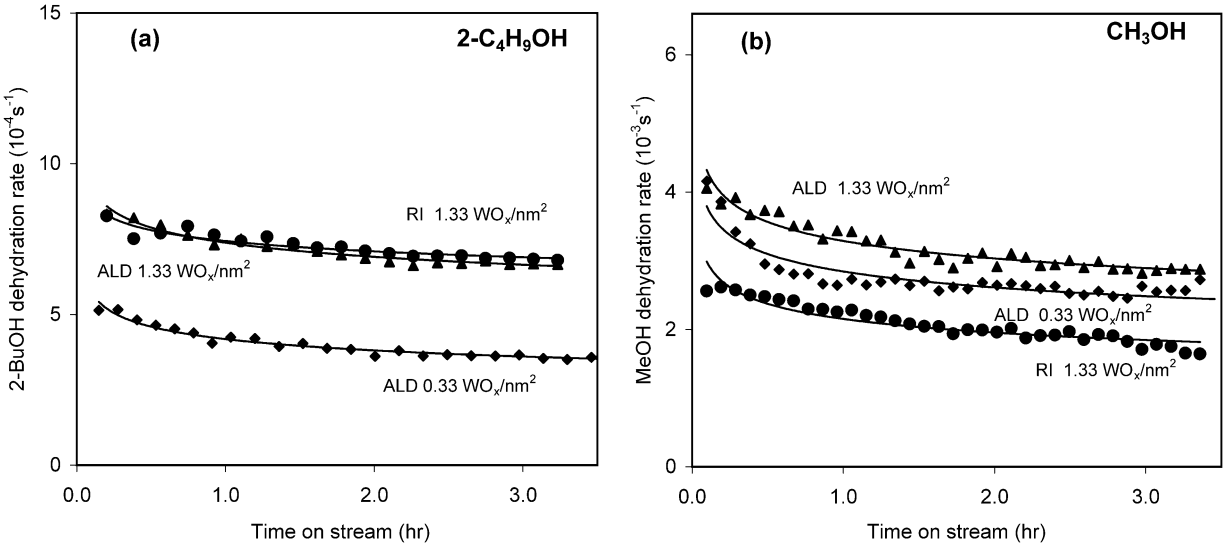

Fig. 9. (a) 2-Butanol dehydration rates (per W-atom) at 373 K as a function of time on stream and WO_x surface density: (◆) ALD 0.33 WO_x/nm^2, (▲) ALD 1.33 WO_x/nm^2, and (●) conventional impregnated 1.33 WO_x/nm^2 (0.5 kPa 2-butanol, 100.8 kPa He, 80 sccm total flow rate). (b) Methanol dehydration rates (per W-atom) at 573 K as a function of time on stream and WO_x surface density: (◆) ALD 0.33 WO_x/nm^2, (▲) ALD 1.33 WO_x/nm^2, and (●) conventional impregnated 1.33 WO_x/nm^2 (1.0 kPa methanol, 100.3 kPa He, 80 sccm total flow rate).

of 2-butanol to ethers was not observed, because such reactions are significantly slower than monomolecular pathways leading to alkenes, especially at low alcohol pressures [28,57,58].

Fig. 9a shows steady-state 2-butanol dehydration rates (per W atom) as a function of time on stream on two samples prepared by ALD with surface densities of 0.33 and 1.33 WO_x/nm^2 and on a sample prepared by impregnation with a surface density of 1.33 WO_x/nm^2. These data show that 2-butanol dehydration rates are strongly influenced by WO_3 content and that optimum rates (per W atom) are achieved at intermediate WO_3 contents, as also shown previously for WO_x species on ZrO_2 [11,28] and Al_2O_3 [29] supports. Rates are similar on the samples with a surface density of 1.33 WO_x/nm^2 prepared by either ALD or impregnation methods and treated at 673 K.

Fig. 9b shows that methanol dehydration rates (per W atom) also depend on WO_3 content, but in this case, the rate is higher on the sample prepared by ALD than on the sample with similar composition but prepared via impregnation. Also, deactivation is more rapid on samples with lower tungsten oxide loadings than on samples with higher densities of WO_x species.

Fig. 10 shows that 2-butanol and methanol dehydration rates (373 and 573 K, respectively) decrease with increasing reactant conversion on a sample with a surface density of 0.66 WO_x/nm^2 prepared by ALD; the conversion can be varied by changing the space velocity. Similar trends are found on all of the other samples. These trends reflect kinetic inhibition by water formed during 2-butanol dehydration [28]. A more rigorous comparison of intrinsic reactivity requires that we extrapolate measured rates to zero reactant conversion; these rates are shown in Fig. 11 as a function of WO_x surface density. The trends observed for 2-butanol dehydration are similar to those reported on WO_x–ZrO_2 [28] and WO_x–Al_2O_3 [29] as a function of WO_x surface density. Samples with low WO_x surface densities and high absorption edge energies (Table 1) appear

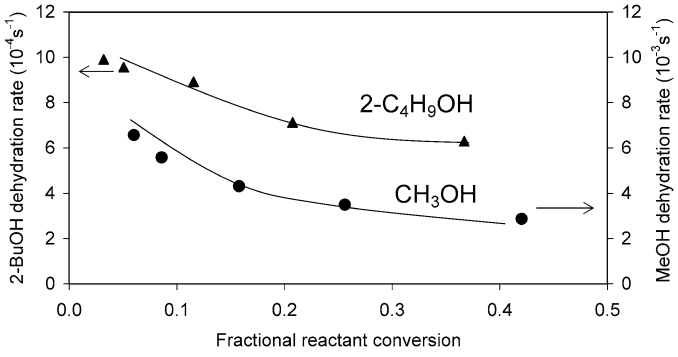

Fig. 10. (▲) 2-Butanol dehydration rates (per W-atom) at 373 K as a function of conversion for an ALD sample with surface density 0.66 WO_x/nm^2 [0.5 kPa 2-butanol, 100.8 kPa He, 6.2–111.3 mol 2-BuOH/(mol W h)]. (●) Methanol dehydration rates (per W-atom) at 573 K as a function of conversion for an ALD sample with surface density 0.66 WO_x/nm^2 [1.0 kPa methanol, 100.3 kPa He, 24.6–394 mol MeOH/(mol W h)].

to contain predominately monotungstate species and show very low catalytic dehydration rates (Fig. 11). Dehydration rates increase as isolated WO_x species condense into polytungstate species with increasing WO_x content. At even higher WO_x content (200% monolayer coverage), dehydration rates decrease as three-dimensional WO_3 crystallites form and WO_x species become inaccessible to reactants. These trends are also seen for methanol dehydration rates, which appear to require similar Brønsted acid sites.

Methanol dehydration rates decrease with time-on-stream more rapidly than 2-butanol dehydration rates (Fig. 9), possibly because of the higher temperatures required for methanol reactions. The presence of water at these higher reaction temperatures (573 K) may cause more rapid sintering of WO_x species or carbon deposition at Brønsted acid sites formed via reduction of W centers [28]. These two factors may account for the different activities observed for methanol dehydration (Figs. 9

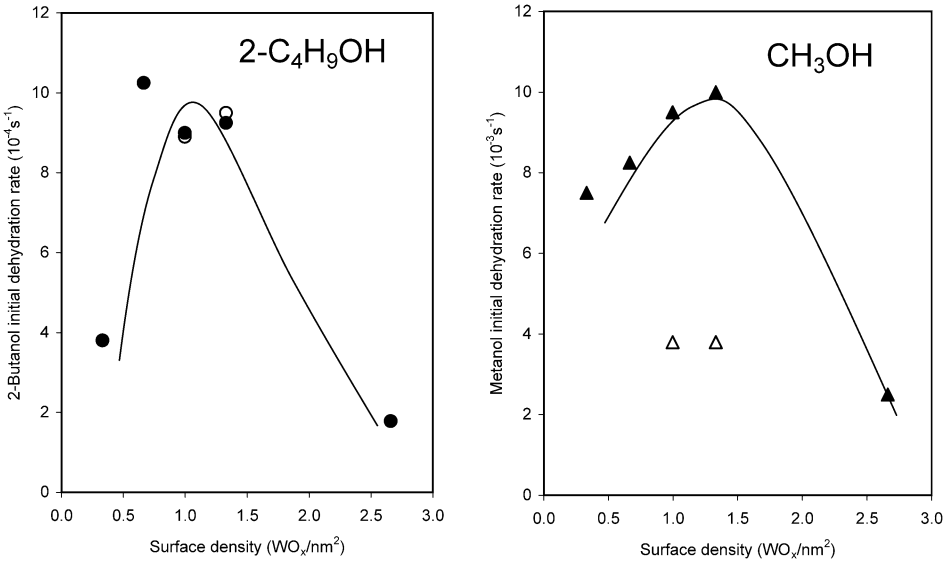

Fig. 11. (Circles) Initial 2-butanol dehydration rates (per W-atom) at 373 K as a function of tungsten oxide surface density in the catalyst. (Triangles) Initial methanol dehydration rates (per W-atom) at 573 K as a function of tungsten oxide surface density in the catalyst. The filled symbols correspond to catalyst obtained by ALD and the open ones to conventionally impregnated samples.

and 11) on samples with identical tungsten loadings but prepared using different methods. The rationale for the observed differences in catalytic behavior between the ALD and impregnated samples and the origin of the deactivation are discussed next based on characterization of spent catalysts.

3.7. TPO

TPO can be used to probe carbonaceous deposits on catalyst surfaces. Analysis of the evolved CO_2/CO allows both qualitative and quantitative assessments of the type and reactivity of these deposits [59,60]. TPO measurements detected significant amounts of carbon after methanol dehydration, but no carbon deposits after 2-butanol dehydration. This indicates that carbonaceous deposits on the catalysts may well be one reason for catalyst deactivation during methanol dehydration.

Fig. 12 compares TPO profiles for two samples with a surface density of 1.33 W/nm^2, prepared by ALD and impregnation, after methanol dehydration at 573 K for 2 h. Both samples show maximum oxidation rates at ∼783 K, but the impregnated samples show an additional strong feature at ∼843 K. These more refractory carbonaceous deposits may reflect an intrinsic difference in acid site strength between these materials. Indeed, MeOH-TPD experiments [61] indicated that samples prepared by ALD and conventional impregnation with the same WO_3 loading (i.e., 1.00 WO_x/nm^2) show a small but clear difference in the temperature at which methoxide species recombinatively desorb as methanol (332 K vs. 346 K for desorption peaks), suggesting that methoxide species are more strongly adsorbed on the impregnated sample. These stronger sites are likely to deactivate more rapidly during the initial reaction stages of reaction and affect the interaction of the dehydrogenation products (formed at the initial stages of the reaction as well) with the surface, thus leading to the formation of more refractory carbon on the catalyst surface. This may account for the differences observed in the two TPO profiles shown in Fig. 12. It is also possible that the crystalline WO_3 phase present on the sample prepared by conventional impregnation overreduces during methanol dehydration, leading to the formation of more refractory carbon. In any case, the total amount of carbon is almost the same in both samples, which seems to indicate that the observed differences in catalytic activity for methanol dehydration between ALD and conventional impregnated samples (Fig. 11b) are not due to the blockage of the catalyst surface by carbonaceous species.

3.8. UV–vis spectra of spent catalysts

Fig. 13 shows the in situ UV–vis spectra of two WO_3/SBA-15 samples (1.33 W/nm^2) prepared by ALD and impregnation as a function of time on stream during 2-butanol dehydration at 423 K. Absorption intensity appears in the pre-edge region as reaction proceeds, reflecting the formation of reduced "color centers" with concurrent generation of Brønsted acid sites via dehydrogenation of 2-butanol during the initial stages of the reaction [28]. Interestingly, in the RI sample (Fig. 13a), the pre-edge appears to plateau as the reaction proceeds, whereas in the ALD sample, a plateau in the intensity of the pre-edge is not observed within the range of time on stream studied. These differences may indicate differing degrees of reduction of the tungsten species as the reaction progresses, with a larger amount of reducible tungsten domains in the case of the ALD sample. However, as mentioned above, differences in activity between these two samples are not observed; this apparent discrepancy can be rationalized in terms of the stability of the catalysts, as explained below.

The results obtained for the edge energy values on these samples merit some additional discussion. The position of the primary absorption edge remains unchanged as the reaction occurs and pre-edge features appear. Thus, the WO_x domain size

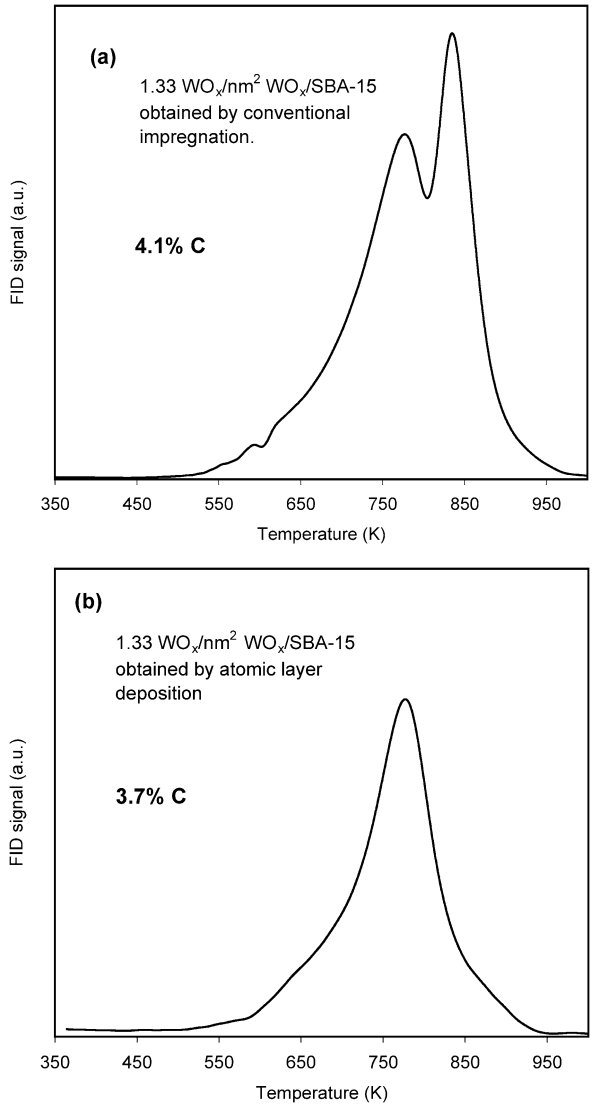

Fig. 12. Temperature-programmed oxidation (TPO) profiles of the carbonaceous species generated after methanol dehydration over (a) a conventionally impregnated sample with surface density 1.33 WO_x/nm^2 and (b) an ALD sample with surface density 1.33 WO_x/nm^2. The profiles were obtained using a mixture of 5% of O_2 in He at a heating rate of 0.2 $K\,s^{-1}$.

remains unchanged by the reaction for both the ALD and conventionally impregnated samples, consistent with the similar 2-butanol dehydration rates on these two samples, which do not sinter during reaction. Nonetheless, studies of these samples before reaction show the presence of crystalline WO_3 only in the impregnated sample. Thus, it appears that impregnated samples have a broader WO_x domain size distribution but an average activity similar to that of the ALD samples, which have a narrower distribution of domain sizes. The similar steady-state activities observed are also related to the mild reaction conditions used to perform 2-butanol dehydration, under which both type of catalysts are stable. Under the more severe reaction conditions needed for methanol dehydration (573 K), differences in the stability and performance between the ALD and conventionally impregnated materials are indeed observed.

Methanol dehydration reactions lead to a decrease in the adsorption edge energy for both ALD and impregnated samples

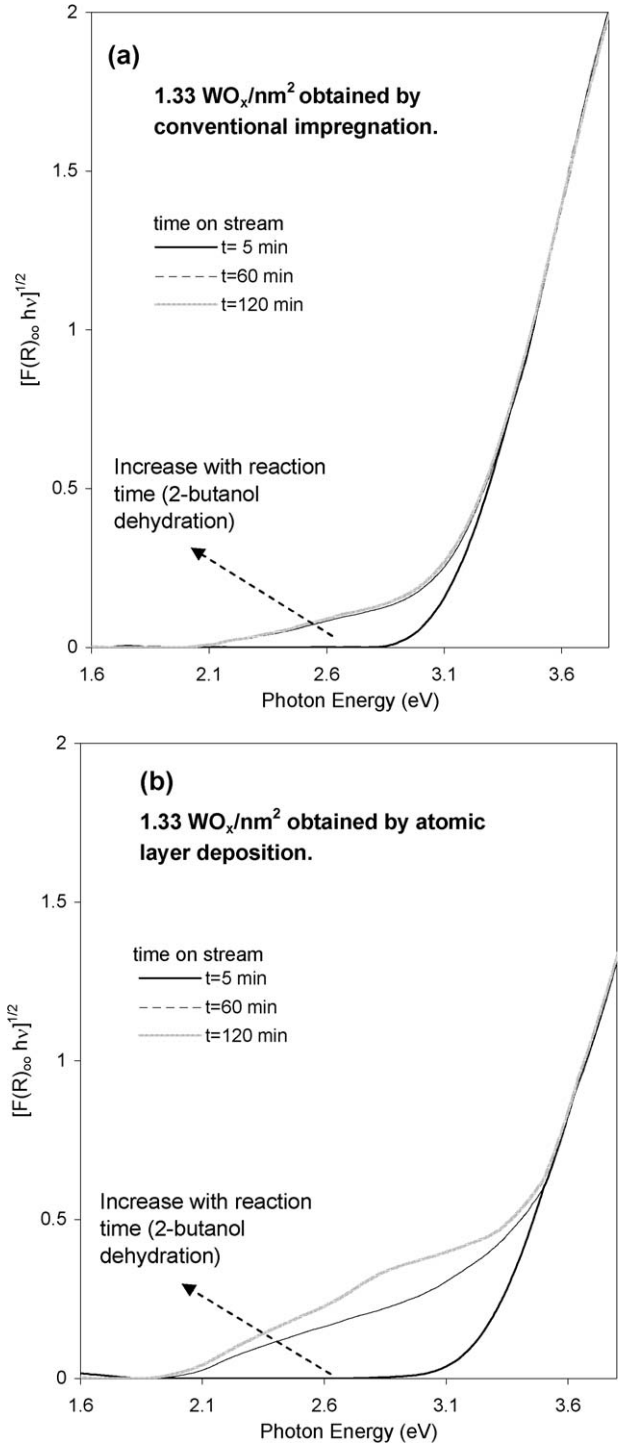

Fig. 13. Diffuse reflectance UV–vis absorption spectra obtained during 2-butanol dehydration on a sample with surface density 1.33 WO_x/nm^2 prepared by (a) conventional impregnation and (b) atomic layer deposition (423 K, 0.5 kPa 2-butanol, 100.8 kPa He, 80 sccm total flow rate). $[F(R_\infty)h\nu]$ represents the Kubelka–Munk function multiplied by the photon energy.

(Fig. 14), indicating that WO_x domains grow during reaction. Pre-edge features for reduced centers are not detectable, because the samples were treated in air at 673 K for 2 h to remove carbon deposits before measuring spectra. WO_x growth occurs rapidly during methanol dehydration, because spectral changes are evident even after only 300 s on stream. It is likely that sin-

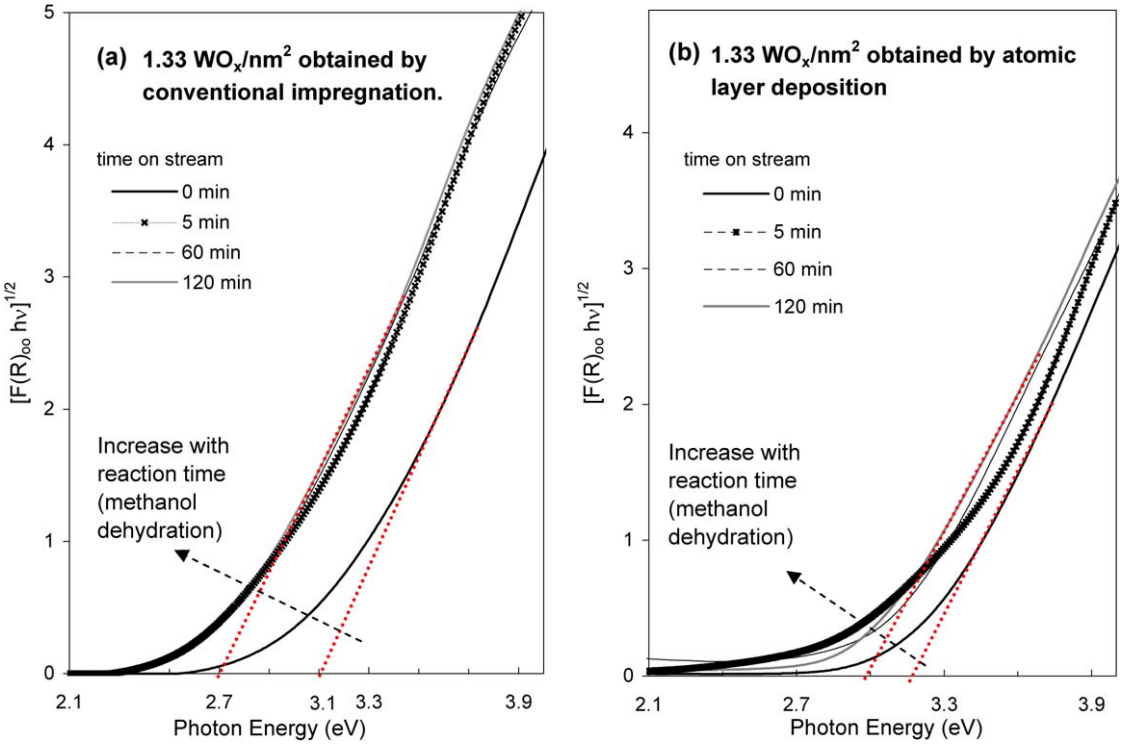

Fig. 14. Diffuse reflectance UV–vis absorption spectra obtained after methanol dehydration on a sample with surface density 1.33 WO_x/nm^2 prepared by (a) conventional impregnation and (b) atomic layer deposition (573 K, 1.0 kPa 2-butanol, 100.3 kPa He, 80 sccm total flow rate). $[F(R_\infty)h\nu]$ represents the Kubelka–Munk function multiplied by the photon energy.

tering accompanies the reduction of WO_x species during initial contact with methanol at 573 K. Moreover, these changes in edge energies are much more pronounced for impregnated samples than for ALD samples (0.2 vs. 0.5 eV shifts; Fig. 14), consistent with the higher apparent methanol dehydration rates on the latter samples (Fig. 11). However, this difference in activity between the ALD and conventionally impregnated samples is not present in the case of 2-butanol dehydration, where the UV–vis DRS results indicate a lack of WO_x sintering. As mentioned above, this difference in catalytic behavior appears to be related to the different reaction conditions used for methanol and 2-butanol reactants. At the higher reaction temperatures required for methanol dehydration, the presence of water vapor (a byproduct of dehydration) is likely to enhance sintering by hydrolyzing the Si–O–W bonds between WO_x and the support and mobilizing tungsten oxide species. The higher resistance to this sintering process of the catalyst prepared by ALD may reflect either a higher density of Si–O–W moieties or a more effective use of the available surfaces area of silica by ALD relative to conventional impregnation methods.

4. Conclusion

Supported tungsten oxide materials synthesized by ALD are very promising catalysts. High dispersions are achieved even at a WO_3 loading of 30 wt%, and enhanced thermal stability is observed, leading to superior catalytic activity for reactions requiring severe conditions, such as methanol dehydration. The differences in activity observed between the samples prepared by ALD and conventional impregnation are attributed mainly to improved resistance toward sintering of the catalyst prepared by ALD, which in turn is rationalized in terms of the higher density of Si–O–W moieties due to a better interaction of WO_x with the support surface. The TPO results reveal that the samples prepared by ALD have a more uniform acid strength compared with the samples prepared by conventional impregnation and that coke formation is not a major factor causing the different steady-state activities in the ALD and impregnated samples for methanol dehydration.

Acknowledgments

This work was supported by US Department of Energy (DOE), Office of Basic Energy Sciences, Division of Chemical Sciences under contract DE-AC06-76RLO-1830 #45385. The research was performed in the Environmental Molecular Sciences Laboratory, a national scientific user facility sponsored by the DOE Office of Biological and Environmental Research and located at the Pacific Northwest National Laboratory. Some of the research was carried out at the Berkeley Catalysis Center facilities of the University of California at Berkeley (UCB). The UCB research was supported by a grant from the DOE, Office of Basic Energy Sciences, Division of Chemical Sciences. The authors thank Professor Daniel Resasco, University of Oklahoma for his help with the TPO profile measurements.

References

[1] L.S. Wang, L.X. Tao, M.S. Xie, G.F. Xu, J.S. Huang, Y.D. Xu, Catal. Lett. 21 (1993) 35.

[2] C.L. Thomas, Catalytic Processes and Proven Catalysts, Academic Press, New York, 1970.
[3] J. Pasel, P. Kassner, B. Montanari, M. Gazzano, A. Vaccari, W. Makowski, T. Lojewski, R. Dziembaj, H. Papp, Appl. Catal. B: Environ. 18 (1998) 199.
[4] A. Butler, C. Nicolaides, Catal. Today 18 (1993) 443.
[5] W.Z. Cheng, V. Ponec, Catal. Lett. 25 (1994) 337.
[6] M.A. Alvarez-Merino, F. Carrasco-Marín, C. Moreno-Castilla, J. Catal. 192 (2000) 374.
[7] C. Moreno-Castilla, M.A. Alvarez-Merino, F. Carrasco-Marín, React. Kinet. Catal. Lett. 71 (2000) 137.
[8] L.L. Murrell, N.C. Dispenziere Jr., Catal. Lett. 4 (1990) 235.
[9] A.F. Perez-Cadenas, C. Moreno-Castilla, F.J. Maldonado-Hodar, J.L.G. Fierro, J. Catal. 217 (2003) 30.
[10] J.C. Vartuli, J.G. Santiesteban, P. Traverso, N. Cardona Martinez, C.D. Chang, S.A. Stevenson, J. Catal. 187 (1999) 131.
[11] D.G. Barton, S.L. Soled, E. Iglesia, Top. Catal. 6 (1998) 87.
[12] D.G. Barton, S.L. Soled, G.D. Meitzner, G.A. Fuentes, E. Iglesia, J. Catal. 181 (1999) 52.
[13] D.G. Barton, M. Shtein, R.D. Wilson, S.L. Soled, E. Iglesia, J. Phys. Chem. B 103 (1999) 630.
[14] G. Busca, Phys. Chem. Chem. Phys. 1 (1999) 273.
[15] P. Carniti, A. Gervasini, A. Auroux, J. Catal. 150 (1994) 274.
[16] J. Bernholc, J.A. Horsley, L.L. Murrell, L.G. Sherman, S. Soled, J. Phys. Chem. 91 (1987) 1526.
[17] V.M. Benitez, C.A. Querini, N.S. Figoli, R.A. Comelli, Appl. Catal. A 178 (1999) 205.
[18] L. Karakonstantis, H. Matralis, Ch. Kordulis, A. Lycourghiotis, J. Catal. 162 (1996).
[19] D.S. Kim, M. Ostromecki, I.E. Wachs, J. Molec. Catal. A: Chem. 106 (1996) 93.
[20] I.E. Wachs, Catal. Today 27 (1996) 437.
[21] J.C. Mol, J.A. Moulijin, J. Mol. Catal. 15 (1982) 157.
[22] C. Martin, O. Malet, G. Solana, V. Rives, J. Phys. Chem. B 102 (1999) 2759.
[23] R. Thomas, E.M. Van Oers, V.H.J. De Beer, J. Medema, J.A. Moulijin, J. Catal. 76 (1982) 241.
[24] S. Soled, L. Murrell, I. Wachs, G. McVicker, Prep.-Am. Chem. Soc., Div. Pet. Chem. 28 (1983) 1310.
[25] S.L. Soled, G.B. McVicker, L.L. Murrell, L.G. Sherman, N.C. Dispenziere Jr., S.L. Hsu, D. Waldman, J. Catal. 111 (1988) 286.
[26] S. Soled, L.L. Murrell, I.E. Wachs, G.B. McVicker, L.G. Sherman, S. Chan, N.C. Dispenziere, R.T.K. Baker, ACS Symposium Series 279 (1985) 165.
[27] W.V. Knowles, E.I. Ross, I.E. Wachs, M.S. Wong, Abstracts of Papers, 228th ACS National Meeting, Philadelphia, PA, August 22–26, 2004 (2004).
[28] C.D. Baertsch, K.T. Komala, Y.-H. Chua, E. Iglesia, J. Catal. 205 (2002) 44.
[29] J. Macht, C.D. Baertsch, M. May-Lozano, S.L. Soled, Y. Wang, E. Iglesia, J. Catal. 227 (2004) 479.
[30] X.-L. Yang, W.-L. Dai, H. Chen, Y. Cao, H. Li, H. He, K. Fan, J. Catal. 229 (2005) 259.
[31] J. Jarupatrakorn, M.P. Coles, T.D. Tilley, Chem. Mater. 17 (2005) 1818.
[32] Z. Zhang, J. Suo, X. Zhang, S. Li, Appl. Catal. A: Gen. 179 (1999) 11.
[33] E. Briot, J.-Y. Piquemal, M. Vennat, J.-M. Bregeault, G. Chottard, J.-M. Manoli, J. Mater. Chem. 10 (2000) 953.
[34] D. Zhao, J. Feng, Q. Huo, N. Melosh, G.H. Fredrickson, B.F. Chmelka, G.D. Stucky, Science 279 (1998) 548.
[35] I.G. Shenderovich, G. Buntkowsky, A. Schreiber, E. Gedat, S. Sharif, J. Albrech, N.S. Golobev, G.H. Findenegg, H. Limbach, J. Phys. Chem. B 107 (2003) 11924.
[36] Y. Wang, Q. Cheng, W. Yang, Z. Xie, W. Xu, D. Huang, Appl. Catal. A: Gen. 250 (2003) 25.
[37] M.H. Lim, A. Stein, Chem. Mater. 11 (1999) 3285.
[38] B.C. Gerstein, C.R. Dybowsky, Transient Techniques in NMR of Solids, Academic Press, San Diego, 1985.
[39] M. Hunger, D. Freude, H. Pfeifer, H. Bremer, M. Jank, K.P. Wendland, Chem. Phys. Letts. 100 (1983) 29.
[40] C.E. Bronnimann, I.S. Chuang, B.L. Hawkins, G.E. Maciel, J. Am. Chem. Soc. 109 (1987) 1562.
[41] J.M. Miller, L.J. Lakshmi, Appl. Catal. A: Gen. 190 (2000) 197.
[42] C.E. Bronnimann, R.C. Zeigler, G.E. Maciel, J. Am. Chem. Soc. 110 (1988) 2023.
[43] S.F. Dec, C.E. Bronnimann, R.A. Wind, G.E. Maciel, J. Magn. Res. 82 (1989) 454.
[44] G.E. Maciel, P.D. Ellis, in: A.T. Bell, A. Pines (Eds.), NMR Techniques in Catalysis, Marcel Dekker, New York, 1994, pp. 231–309.
[45] J.Z. Hu, J.H. Kwak, J.E. Herrera, Y. Wang, C.H.F. Peden, Solid State Nucl. Magn. Reson. 27 (2005) 200.
[46] A. Gutiérrez-Alejandre, P. Castillo, J. Ramirez, G. Ramis, G. Busca, Appl. Catal. A: Gen. 216 (2001) 181.
[47] A. Khodakov, J. Yang, S. Su, E. Iglesia, A.T. Bell, J. Catal. 177 (1998) 343.
[48] D. Wei, G.L. Haller, Proceedings of the 2nd Memorial G.K. Boreskov International Conference, Novosibirsk, July, 1997, p. 110.
[49] E.A. Davis, N.F. Mott, Philos. Mag. 22 (1970) 903.
[50] R.S. Weber, J. Catal. 151 (1995) 470.
[51] M. Fournier, C. Louis, M. Che, P. Chaquin, D. Masure, J. Catal. 119 (1989) 400.
[52] H. So, M.T. Pope, Inorg. Chem. 11 (1972) 1441.
[53] M.L. Good, Spectrochim. Acta A 29 (1973) 707.
[54] M. Iwamoto, H. Furukawa, K. Matsukami, T. Takenaka, S. Kagawa, J. Amer. Chem. Soc. 105 (1983) 3719.
[55] E. Iglesia, D.G. Barton, S.L. Soled, S. Miseo, J.E. Baumgartner, W.E. Gates, G.A. Fuentes, G.D. Meitzner, Stud. Surf. Sci. Catal. 101 (1996) 533.
[56] D. Masure, P. Chaquin, C. Louis, M. Che, M. Fournier J. Catal. 119 (1989) 415.
[57] H. Knozinger, R. Kohne, J. Catal. 5 (1966) 264.
[58] H. Knozinger, H. Buhl, K. Kochloefl, J. Catal. 24 (1972) 57.
[59] D.E. Resasco, B.K. Marcus, C.S. Huang, V.A. Durante, J. Catal. 146 (1994) 40.
[60] S.M. Stagg, C.A. Querini, W.E. Alvarez, D.E. Resasco, J. Catal. 168 (1997) 75.
[61] J.H. Kwak, J.E. Herrera, Y. Wang, C.H.F. Peden, manuscript in preparation.